CHEMISTRY OF MATERIALS

Article

pubs.acs.org/cm

Restructuring of AuPd Nanoparticles Studied by a Combined XAFS/DRIFTS Approach

Emma K. Gibson,*[,†,‡] Andrew M. Beale,[†,‡] C. Richard A. Catlow,[†,‡] Arunabhiram Chutia,[†,‡] Diego Gianolio,[§] Anna Gould,[†,‡] Anna Kroner,[§] Khaled M. H. Mohammed,[†,‡,∥] Michal Perdjon,[†,‡] Scott M. Rogers,[†,‡] and Peter P. Wells*[,†,‡]

[†]UK Catalysis Hub, Research Complex at Harwell, Rutherford Appleton Laboratory, Harwell Oxon, Didcot OX11 0FA, United Kingdom

[‡]Department of Chemistry, University College London, 20 Gordon Street, London WC1H 0AJ, United Kingdom

[§]Diamond Light Source Ltd, Harwell Science and Innovation Campus, Chilton, Didcot OX11 0DE, United Kingdom

[∥]Chemistry Department, Faculty of Science, Sohag University, Sohag, P.O.B 82524, Egypt

Supporting Information

ABSTRACT: The use of AuPd nanoparticles in catalysis is widespread, with the activity being attributed to their precise structural properties. We demonstrate the restructuring of AuPd nanoparticles under CO oxidation conditions using a combined XAFS/DRIFTS approach. The fresh catalyst exhibits PdO islands at the surface of the nanoparticles, which are reduced under reaction conditions, a process observed via both DRIFTS and Pd K-edge XAFS measurements. From the EXAFS analysis alone the nanoparticles were observed to have a Au rich core with an outer region of intimately mixed Au and Pd atoms. This structure was found to remain mostly unaltered throughout reaction. However, the DRIFTS spectra showed that although Au was present on the surface during the initial stages of reaction the surface rearranged just before light-off, and contained only Pd atoms thereafter. This study highlights the advantage of this combined approach, where both the surface structure and local environment of the constituent metals can be probed simultaneously, allowing a complete picture of the restructuring of these bimetallic particles to be obtained under reaction conditions.

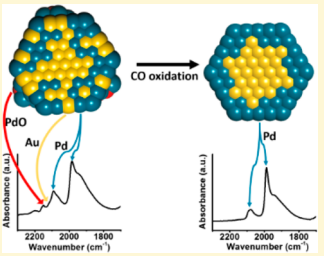

INTRODUCTION

The addition of Pd to Au to produce bimetallic catalysts is advantageous for many catalytic processes. The industrial production of vinyl acetate[1,2] is one example, with many other reactions, such as glycerol oxidation,[3] the formation of H_2O_2 from H_2 and O_2[4] and the oxidation of alcohols to aldehydes currently being investigated.[5]

Monometallic Au catalysts are well-known for their high activity for the oxidation of CO at low temperatures,[6] although it has been previously stated that there is limited understanding of this high activity.[7] The effect which particle size, support interaction and the oxidation state of Au have on the activity of Au catalysts for the oxidation of CO are not well understood.[7] However, it has recently been shown that the active site for CO oxidation over Au/TiO_2 catalysts is at the Au-support interface, with O_2 dissociation occurring when adsorbed on a dual Ti Au site.[8] In the case of bimetallic catalysts, the addition of Pd can provide increased activity compared to a monometallic Au catalyst for some reactions, such as glucose oxidation and the direct synthesis of H_2O_2.[9,10] For CO oxidation, the addition of Pd is reported to aid O_2 dissociation and can (in some cases) produce catalysts that are more stable and more active at low temperature than their Au and Pd monometallic counterparts.[11] In addition to the already complex activity of monometallic Au catalysts, the addition of a secondary metal poses even greater challenges in determining accurate structure−function relationships. Bimetallic catalysts are known to restructure under reaction conditions.[12] In the case of model Au−Pd alloy surfaces, increasing CO pressures leads to the segregation of Pd atoms to the surface due to the stronger binding energy of CO to Pd than to Au.[13] In such cases, studying the catalyst under operando conditions becomes essential.

CO adsorption measured by DRIFTS (diffuse reflectance infrared Fourier transform spectroscopy) is a useful technique to characterize the surface of supported metal catalysts and has also been employed to study AuPd bimetallic catalysts;[11,14−16] When combined with XAFS (X-ray absorption fine structure), not only can the surface species be probed, but the oxidation and local coordination of both metals can also be studied providing valuable insights into the reactive species. The combination of XAFS and DRIFTS, first developed by Evans and Newton,[17] has been used to study CO and NO cycling over Rh and Pd automotive emission catalysts and methane oxidation over Pt/Al_2O_3.[18] Recently XAFS/DRIFTS has also been used to study CO oxidation over Pd/Al_2O_3.[19] In the present study, for the first time we have combined the use of

Received: March 6, 2015
Revised: April 15, 2015
Published: April 27, 2015

DOI: 10.1021/acs.chemmater.5b00866
Chem. Mater. 2015, 27, 3714−3720

XAFS and DRIFTS to probe the restructuring of AuPd bimetallic particles under relevant reaction conditions. This work highlights the changeable nature of catalyst structures and the need for advanced combined spectroscopic techniques to link accurately structure to reactivity.

EXPERIMENTAL SECTION

Synthesis. A standard sol-immobilization method with temperature control was used in the preparation of supported AuPd bimetallic nanoparticles.[20] $HAuCl_4{\cdot}3H_2O$ (1.8×10^{-4} M, 99.9%, Alpha-Aesar) and K2PdCl4 (3.3×10^{-4} M, 99.9%, Alpha-Aesar) precursors was used to prepare solutions with the desired gold and palladium concentrations, to which a solution of poly(vinyl alcohol) (PVA, 1 wt % solution, Aldrich, M_w = 9000−10 000 g mol^{-1}, 80% hydrolyzed, PVA/metal (w/w) = 1.2) was added. $NaBH_4$ solution (0.1 M, > 96%, Aldrich, NaBH4/metal (mol/mol) = 5) was added dropwise during stirring to form a sol. After the complete reduction of gold and palladium species (30 min), the colloidal solution was immobilized on to γ-Al2O3 (Degussa, AEROXIDE, AluC) under vigorous stirring conditions. The amount of support material required was calculated so as to have a final metal loading of ∼2.5 wt % of each metal. The mixture was acidified to pH 1−2 by sulfuric acid before it was stirred for 60 min. The slurry was filtered, washed thoroughly with distilled water, and dried overnight. The catalyst was dried at 120 °C for 8 h, then calcined at 300 °C for 8 h.

TEM-EDX. The sample was prepared for TEM and energy-dispersive X-ray analysis (EDX) by dispersing the catalyst powder in high-purity ethanol using ultrasonication. 40 μL of the suspension was dropped on to a holey carbon film supported by a 300 mesh copper grid before the solvent was evaporated. The samples were then examined using a JEOL JEM 2100 EM model.

XAFS-DRIFTS Measurements. XAFS measurements were performed at the Pd K-edge and Au L_3-edge on the B18 beamline at the Diamond Light Source, Didcot, UK. Measurements were performed in transmission mode using a QEXAFS setup with fast-scanning Si (311) and (111) double crystal monochromators for the respective Pd and Au edges. The time resolution of the spectra reported herein was 90s/spectrum (k_{max} = 14.8). A DaVinci arm fitted with Praying Mantis Optics was used to refocus the IR beam outside the FTIR spectrometer so that the X-ray beam could be transmitted through the DRIFTS cell.

The samples were placed in the Harrick X-ray transmission DRIFTS cell attached to the end of the DaVinci arm. The arm has motorized stages able to move vertically and horizontally by 48 mm, enabling ease of alignment of the DRIFTS cell in the X-ray beam. The cell is fitted with glassy carbon windows for exit and entry of the X-ray beam and ZnSe windows for collection of DRIFTS spectra. The XAFS/DRIFTS cell which has been described in detail elsewhere,[21] has an X-ray path length of 3.17 mm placed 1.04 mm below the surface of the catalyst. DRIFTS spectra were collected with an Agilent Carey 680 FTIR spectrometer taking 64 scans with a resolution of 4 cm^{-1} using the liquid nitrogen cooled MCT detector.

The sample was first heated to 130 °C and held for 10 min under a flow of He to remove adsorbed water from the sample. After which, the sample was cooled to room temperature where a series of 5 XAFS spectra and an infrared spectrum were recorded. The sample was then ramped at 3°/min to 350 °C and then cooled to room temperature under a constant flow of 12.5 mL/min CO in He (10%) and 12.5 mL/min O_2 in He (10%). During reaction and cooling both XAFS at the Pd K-edge and DRIFTS spectra were collected continuously, with spectra obtained every 90s and 30s, respectively. The reaction was then repeated at the Au L_3-edge using a fresh sample, for both the Au and Pd experiments the appropriate foil was placed between I_t and I_{ref}. The outlet gas was monitored using a MKS mass spectrometer.

EXAFS (Extended X-ray Absorption Fine Structure) Analysis. All XAFS spectra were acquired concurrently with the appropriate foil placed between I_t and I_{ref}. XAFS data processing was performed using IFEFFIT[22] with the Horae package[23] (Athena and Artemis). The amplitude reduction factor, S_0^2 was derived from EXAFS data analysis of the Pd foil and Au foil reference spectra, (with known coordination numbers which were fixed during analysis). The values obtained were 0.85 and 0.83 for Pd and Au. Respectively. These values were used as fixed input parameters in the fits. The increase with temperature of the σ^2 value, the mean-square relative displacement of absorber and backscatter atoms, was estimated based on the method described elsewhere for the change in the σ^2 value with increasing temperature.[24] The same rate of change in σ^2 with temperature was applied to the spectra collected during the CO oxidation experiment but starting from the σ^2 values determined from the fits of the spectra collected at 25 °C at the Pd K-edge and Au L_3-edge. This is described in more detail in the Supporting Information.

RESULTS

TEM-EDX. One of the TEM images and the derived histogram for the 100 particles measured are shown in Figure 1.

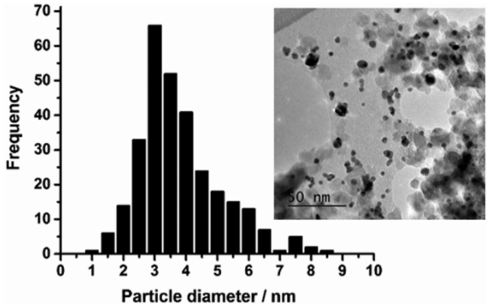

Figure 1. Particle size histogram from the TEM analysis and a representative image.

The average size of the AuPd particles was found to be 4.1 ± 1.3 nm. EDX point measurements were taken over 10 particles chosen at random; each particle was found to contain both Au and Pd.

XANES. The X-ray absorption near edge structure (XANES) spectra (Figure 2) collected during the Pd K-edge experiment shows that the Pd environment of the initial catalyst is broadly consistent with PdO, as discussed below.[25] The Pd is reduced by 152 °C, shown in blue in Figure 2, then appears to start to reoxidize from 263 °C after light-off, shown in red in Figure 2. On cooling the catalyst is once again reduced and remains in

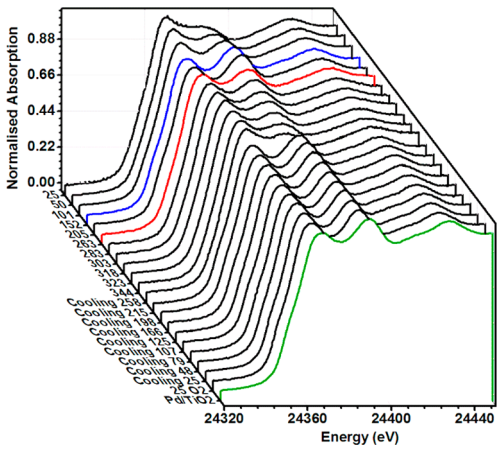

Figure 2. Normalized XANES Spectra at the Pd K-edge during CO oxidation, ramping from RT to 350 °C then cooling to RT. The Pd/TiO_2 reference is shown in green, the spectra recorded at 150 and 263 °C are shown in blue and red, respectively.

DOI: 10.1021/acs.chemmater.5b00866
Chem. Mater. 2015, 27, 3714−3720

this state even under O_2 at room temperature demonstrating that the catalyst is stable in its reduced form.

Evidence of the initial reduction is shown by the shift of the edge position by 1 eV to lower energy and a reduction in intensity of the first feature after the edge, at 24368 eV; both changes are consistent with reduction to Pd metal. The XANES spectrum of a Pd/TiO_2 catalyst with approximately 1.4 nm particles, similar in size to those of the $AuPd/Al_2O_3$ studied here is shown in green in Figure 2 for comparison. After light-off, at 263 °C shown in the mass spectrum in Figure 3, the

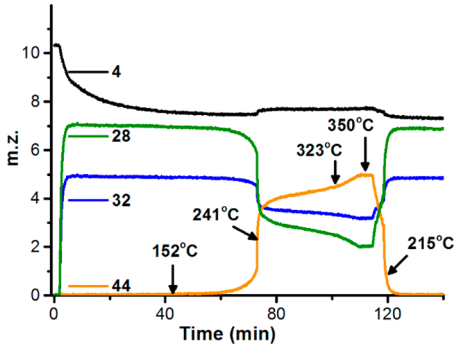

Figure 3. Mass spectrometry data for the combined XAFS DRIFTS experiments. Masses 4, 28, 32, and 44 represent He, CO, O_2, and CO_2, respectively. Mass 28 has been corrected for the contribution from CO2.

XANES features begin to change and by 344 °C the edge has shifted by 0.5 eV toward the initial 25 °C spectrum and the intensity of the feature at 24368 eV increases, consistent with oxidation. This apparent "reoxidation" is discussed in the EXAFS Analysis section below. The reduction observed on cooling is evidenced by the shift of the edge by 1.6 eV to lower energy, from the initial 25 °C spectrum and again a decrease in intensity of the feature at 24368 eV.

When the experiment was repeated on a fresh sample at the Au L_3-edge, little change in the XANES spectra was observed during reaction, as can be seen in Figure 4. However, some conclusions about the extent of alloying can be inferred.

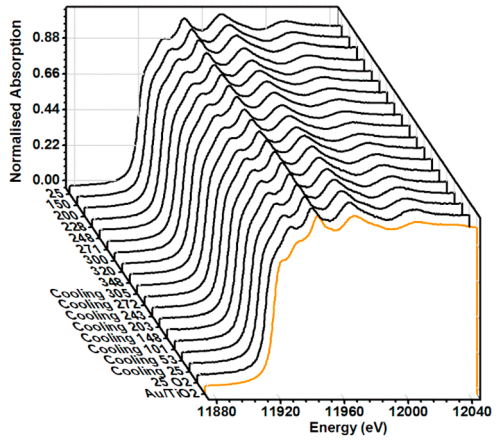

Figure 4. Normalized XANES Spectra at the Au L_3-edge during CO oxidation, ramping from RT to 350 °C then cooling to RT. The XANES spectrum of Au NP's supported on TiO_2 are shown as a reference for reduced Au, these are of similar size (2.8 nm) to the Au NP's in the $PdAu/Al_2O_3$ sample.

A weak white line is observed at 11923 eV that is typical for nanoparticles and is due to electron transition from the 2p to the unoccupied 5d orbitals. In bulk Au systems, this transition is due to overlap of the s, p, and d bands resulting in a slight depletion of the 5d orbitals.[26] Compared to the Au/TiO_2 reference spectrum of 2.8 nm Au particles, the white line in the $AuPd/Al_2O_3$ catalyst is weaker which can be due to smaller particles.[27] However, as the AuPd particles are larger it is probably due to filling of the Au d-band by electron transfer from the Pd atoms.[28] Further evidence of alloying is the greater intensity of the feature at 11934 eV compared to the Au only reference catalyst; this increase in intensity has previously been observed for AuPd bimetallic systems.[28]

EXAFS Analysis. The EXAFS analysis confirms the reduction of PdO to Pd^0 observed in the XANES spectra, followed by a segregation of Pd from the core to the surface at higher temperatures, indicating the restructuring of the catalyst to form a Pd rich shell.

Figure 5 shows the nonphase-corrected Fourier transform of the k^2 weighted Pd K-edge EXAFS data (plus imaginary components of the data and scattering paths) of the sample at 25, 152, and 324 °C. The latter is a merge of several spectra recorded between 303 and 344 °C, in order to improve data quality. The EXAFS fitting parameters are shown in Table 1. For the spectrum taken at room temperature under reaction gases, the data are fitted well using three paths of PdO, Pd−O and two Pd−Pd paths, in addition to a Pd−Au and a Pd−Pd path consistent with Pd metal. These paths are named O(PdO), Pd(PdO), Pd2(PdO), Au, and Pd(Pd) respectively in Table 1. This latter scattering path has a distance of 2.86 Å, which is slightly longer than expected for Pd^0. However, similar R values have been obtained for AuPd nanostructures where the long Pd−Pd distance was attributed to surface relaxation, and so can be a sign that the Pd atoms are mostly at the surface.[29] Another possible cause for this longer R_{Pd-Pd} distance is that the Pd−Pd distance of Pd^0 and that of PdO at 3.07 Å cannot be easily resolved; in fact, these two scattering paths are out of phase with each other as can be seen in Figure 5A.

On heating the sample to 150 °C, the contributions from PdO disappear, and the spectra can be fitted using only the Pd−Pd and Pd−Au scattering paths, consistent with the reduction of the PdO. During this reduction step, the coordination to metallic Pd increases from 5 to 7 and the coordination to Au increases from 2 to 4. As the temperature increases further to 263 °C, a contribution from a low *z*-number element is again observed, which was assumed from the XANES spectra to be reoxidation of the Pd to PdO. However, as no contribution from a Pd distance at ∼3 Å was observed, it is assumed that this contribution is not due to PdO but from either adsorbed O or C. Another possibility would be the formation of a PdC_x phase previously observed by in situ XRD and XAFS/DRIFTS measurements during CO adsorption on Pd.[30] On cooling, as the production of CO_2 decreases (Table S2 in the Supporting Information), the contribution from this O or C was removed after which, no further change in coordination numbers were observed. Further evidence of restructuring of the AuPd NPs can be derived from the changes in Pd−Pd and Pd−Au coordination. From 205 °C a decrease in Pd−Pd coordination and an increase in Pd−Au coordination is observed which may indicate the segregation of Pd from the core to the surface of the particles, as the surface atoms have a lower number of neighbors.[31]

DOI: 10.1021/acs.chemmater.5b00866
Chem. Mater. 2015, 27, 3714−3720

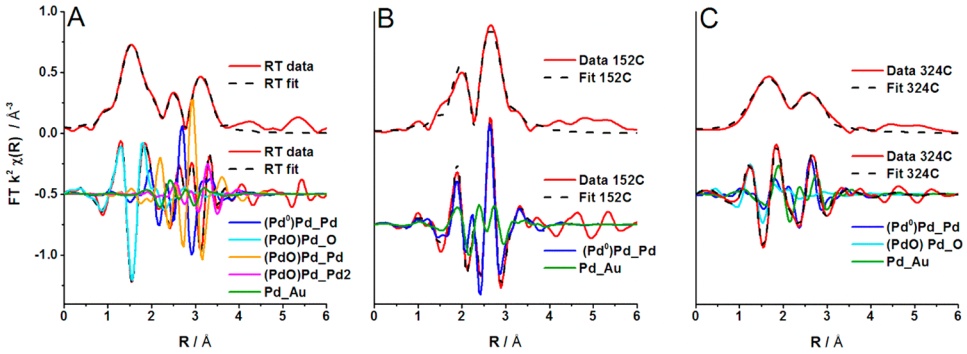

Figure 5. Pd K-edge EXAFS data taken at (A) RT, (B) 152, and (C) 324 °C, showing the magnitude and imaginary components of the k^2 weighted Fourier transform data and fits and the imaginary components of each scattering path used in the fits.

Table 1. EXAFS Fitting Parameters for the Pd K-Edge for Spectra Collected Approximately Every 50 °C during the Temperature Ramp under CO Oxidation Conditions[a]

refined parameter	RT	50 °C	101 °C	152 °C	205 °C	263 °C	289 °C[b]	324 °C[b]
$CN_{Pd(Pd)}$	5(1)	7(1)	8(1)	7(1)	7(1)	5(1)	4.3(4)	3.5(6)
$CN_{O(PdO)}$	2.4(2)	1.9(3)	1.1(3)	0.6(2)	0.9(2)	1.3(3)		
$CN_{Pd(PdO)}$	8(3)	8(2)	5(3)					
$CN_{Pd2(PdO)}$	4(1)							
CN_{Au}	2(2)	3(2)	3(2)	4(1)	4(1)	5(1)	5(1)	5(1)
$R_{Pd(Pd)}$	2.86(4)	2.84(4)	2.79(3)	2.74(1)	2.75(1)	2.72(2)	2.69(2)	2.67(2)
$R_{O(PdO)}$	2.04(2)	2.02(3)	1.98(3)	1.94(3)	1.97(2)	1.95(2)		
$R_{Pd(PdO)}$	3.07(3)	3.06(4)	3.01(4)					
$R_{Pd2(PdO)}$	3.43(3)							
R_{Au}	2.83(7)	2.82(7)	2.78(5)	2.75(3)	2.76(3)	2.75(3)	2.72(2)	2.71(2)
E_0	9(3)	6(2)	6(3)	2(1)	4(1)	2(1)	−2(1)	−3(1)
R-factor	0.0035	0.0038	0.027	0.027	0.034	0.026	0.004	0.016

[a]Fitting parameters: $S_0^2 = 0.85$ as determined by the use of a Pd foil standard; Fit range $3 < k < 10$, $1.15 < R < 3.85$; number of independent points = 11.8. [b]Fitting parameters: $1.15 < R < 3.6$, $3.0 < k < 8.5$, number of independent points = 8.4.

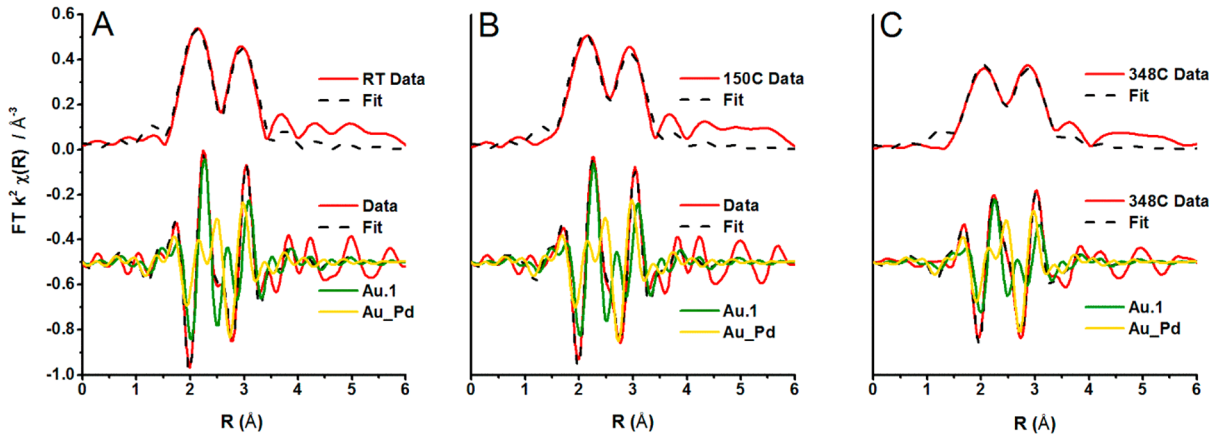

Figure 6. Au L_3-edge EXAFS data taken at (A) RT, (B) 150, and (C) 348 °C, showing the magnitude and imaginary components of the k^2-weighted Fourier transform data and fits and the imaginary components of each scattering path used in the fits.

EXAFS analysis from the Au experiment also provides evidence of restructuring, with Au atoms segregating toward the core on heating. Determination of the short-range order parameter for each metal and evaluation of the generalized Ramsauer−Townsend (GRT) effect[32] indicates that by 150 °C an alloy-like structure exists, whereas on increasing temperature and then on cooling the nanoparticles have evolved to a more core−shell structure. This could be imagined as a gradual segregation of the Pd atoms to the surface and the Au atoms to the core throughout the reaction. The EXAFS data (Figure 6) and fitting parameters for the Au experiment are shown in Table 2 and Table S4 in the Supporting Information.

The segregation of Au from the surface to the core is implied from the increase in Au coordination from 6 to 8 on increasing temperature to 150 °C. In contrast, the Au−Pd coordination is much smaller and little change is observed throughout the reaction. A strong indication of a Au-rich core, Pd shell structure comes from comparison of the total Au-metal and Pd-metal coordination numbers. Above 150 °C the total coordination of gold to metal atoms (Au and Pd) is slightly

DOI: 10.1021/acs.chemmater.5b00866
Chem. Mater. 2015, 27, 3714−3720

Table 2. EXAFS Fitting Parameters for the Au L_3-Edge for Spectra Collected Approximately Every 50 °C during the Temperature Ramp under CO Oxidation Conditions[a]

refined param	RT	58 °C	94 °C	150 °C	200 °C	228 °C	248 °C	271 °C	300 °C	320 °C	348 °C
CN_{Au-Au}	6 (2)	7(1)	7(1)	8(1)	8(2)	7(1)	7(1)	7(1)	7(1)	6(1)	6(1)
CN_{Au-Pd}	4(3)	4(1)	4(1)	4(1)	4(1)	5(1)	4(1)	4(1)	4(1)	4(1)	4(1)
R_{Au-Au}	2.81(4)	2.80(2)	2.81(2)	2.82(2)	2.79(2)	2.80(3)	2.81(3)	2.81(3)	2.81(3)	2.80(3)	2.79(3)
R_{Au-Pd}	2.79(4)	2.79(3)	2.78(3)	2.78(3)	2.76(3)	2.77(3)	2.76(4)	2.76(3)	2.77(4)	2.76(3)	2.76(3)
E_0	3(2)	5(1)	5(2)	5(2)	4(1)	4(2)	4(2)	4(2)	4(2)	4(2)	4(2)
R-factor	0.024	0.0269	0.0307	0.034	0.022	0.042	0.054	0.033	0.041	0.049	0.043

[a]Fitting parameters: $S_0^2 = 0.83$ as determined by the use of a Au foil standard; fit range $3 < k < 8.5$, $1.15 < R < 4$; number of independent points = 9.8.

greater than the total coordination of Pd to metal atoms. Confirmation of these Au-rich cores comes from the observed higher Au−Au coordination than the Au−Pd coordination.[14] However, as the coordination to Pd is not insignificant a sizable proportion of the Au atoms must be in contact with the Pd, therefore we propose that there is a gradient between the Pd shell and Au core. A more in depth scrutiny of the coordination numbers can be performed by calculating the Cowley short-range order parameter, α, as described in references 29a and b.[33,34] The α-values calculated for Au and Pd for the data collected at 150 °C and on cooling (Table S5 in the Supporting Information) are consistent with alloy and core−shell type structures, respectively.[34] This is described in greater detail in the Supporting Information. Further confirmation of the change from alloy to core−shell structure comes from the GRT effect. A π phase flip of the backscattering wave at $k = 6$ Å^{-1} occurs for elements of atomic number greater than 78 and results in a peak in the Fourier transform at very low *r*, too short to be due to an actual chemical bond. In the case of AuPd bimetallic particles, the intensity of this peak would increase with increasing number of bimetallic bonds, because $Z_{Au} = 79$. However, a slight decrease in intensity is observed on increasing temperature for the AuPd NPs, Figure 6, consistent with a change from an alloy to a more core−shell type structure.

DRIFTS. Surface adsorbates were monitored during reaction by DRIFTS; the spectra recorded during the experiment performed at the Pd K-edge are shown in Figure 7. The DRIFTS spectra confirm the reduction of PdO to Pd by 150 °C, as observed in the Pd XANES spectra, with the loss of the bands observed at 2157 and 2137 cm^{-1} which can be assigned to CO adsorbed on Pd^{2+} and Pd^{+} of PdO.[35] As the bands due to PdO decrease, a shoulder at 2115 cm^{-1} becomes visible, which can be tentatively assigned to CO adsorbed on Au^0.[7,14,36] This band becomes visible at 101 °C and disappears by 175−200 °C, as shown in Figure S5 in the Supporting Information. This observation is consistent with the Au EXAFS analysis which implied a restructuring of the Au atoms toward the core on increasing temperature. In order to investigate the presence of CO adsorbed on Au sites in more detail a temperature-programmed desorption measurement followed by DRIFTS was performed; the resulting spectra are shown in Figures S6 and S7 of the Supporting Information. As no reaction was occurring during the increase in temperature, the different CO adsorption bands could be more easily assigned. A band is observed at 2109 cm^{-1} which desorbed by 95 °C, which can be assigned to CO on Au^0. Another band at 2123 cm^{-1} was also observed, but this desorbs after only 3 min at room temperature under flow of He and can be attributed to CO adsorbed on $Au^{\delta+}$.[14]

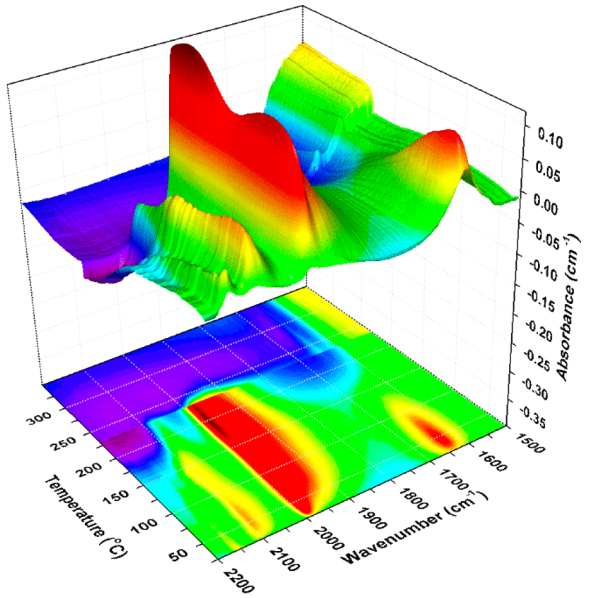

Figure 7. DRIFTS spectra taken during the ramp to 350 °C in the Pd K-edge experiment.

Infrared bands consistent with linear adsorbed CO on Pd, bridge-bonded CO on Pd and CO on Pd 3-fold sites were observed at 2090, 1990, and 1930 cm^{-1}.[37] The fact that CO can adsorb on 3-fold Pd sites is indication that the surface is not a well-mixed Au−Pd system but is Pd-rich.[16] The poor activity of the catalyst at low temperatures is also indication of the Pd rich surface, as Au is expected to be active for CO oxidation at room temperature. However, this activity is proposed to be reliant on Au edge and corner sites.[16,38] The in-activity of our catalyst at RT could be explained by the occupation of these sites by Pd atoms. At 125−150 °C as the PdO is reduced, the linear and bridged CO adsorbed on Pd increase in intensity. After light-off, at approximately 240 °C, no further surface adsorbates can be observed in the DRIFTS spectra; this phenomena has previously been investigated by XPS, where the surface was heated in the presence of CO and O_2. These measurements showed the abruptness of the switch from adsorbed CO (533 eV) to adsorbed atomic oxygen (530 eV), which occurs at the temperature of light-off.[39] On cooling to 325 °C surface adsorbed species, namely CO adsorbed on Pd, could again be observed. During this cooling stage (Figure S8 in the Supporting Information), no CO adsorbed on Pd^{2+} or Pd^{+} was observed, in agreement with the XAFS results which showed that no reoxidation of the catalyst occurred. On cooling and under O2 at RT there is no evidence of Au at the surface; the band for CO adsorbed on Au at 2110 cm^{-1} is not observed,

DOI: 10.1021/acs.chemmater.5b00866
Chem. Mater. 2015, 27, 3714−3720

suggesting that after reaction the surface of the nanoparticles is covered solely by Pd.

CONCLUSIONS

The information obtained from each technique is complementary and allows us to build a complete picture of the restructuring of these bimetallic nanoparticles. The reduction of PdO is observed from the Pd XANES spectra and via the position of the infrared bands of the adsorbed CO species. Furthermore, the partitioning of Au atoms from the surface to the bulk during reaction could only be implied from the EXAFS analysis but is confirmed from the DRIFTS measurements. This combination of techniques has allowed us to follow the restructuring of these bimetallic nanoparticles under reaction conditions. Figure 8 illustrates this restructuring with images A and B showing the fresh catalyst at RT containing a Au rich core with a AuPd alloy layer and a surface containing PdO islands, and images C and D showing the final state of the catalyst which we propose maintains the gold rich core and AuPd alloy layer but has a skin of Pd at the surface. We note that Figure 8 is meant as an illustration only and not an accurate representation of the coordination numbers determined from the EXAFS analysis.

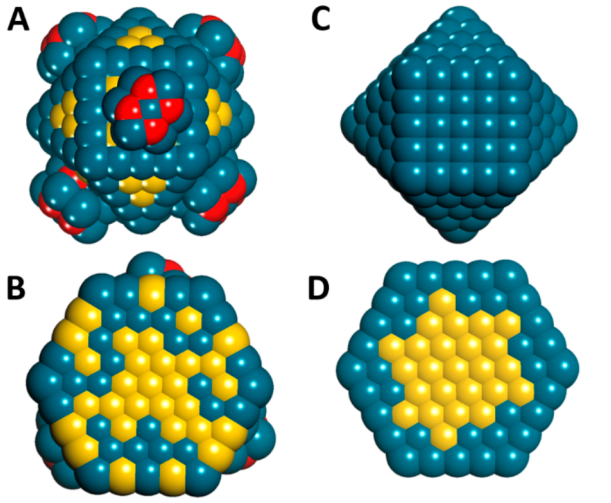

Figure 8. Schematic representation of (A) the fresh catalyst, (B) the cross-section of the fresh catalyst, (C) the final catalyst state after reaction, and (D) the cross-section of the final catalyst, where the red, blue, and yellow balls indicate O, Pd, and Au atoms, respectively.

The application of XAFS can greatly help understand the local structure of bimetallic catalysts under reaction conditions. However, being an averaging technique, it can sometimes provide limited information about the surface. When used in combination with FTIR, an understanding of both the local structure of the metals as well as the surface species can be achieved. In the case of CO oxidation over AuPd nanoparticles, the restructuring of the particles during reaction was observed.

ASSOCIATED CONTENT

Supporting Information

TEM results, details of the determination of the σ^2 value, the full tables of the EXAFS fitting parameters for the ramp and cooling of the experiments at both Pd K and Au L_3-edges, determination of the Cowley short-range order parameter, DRIFTS spectra obtained for the CO TPD measurement and the DRIFTS spectra recorded during the cooling stage of the CO oxidation reaction. The Supporting Information is available free of charge on the ACS Publications website at DOI: 10.1021/acs.chemmater.5b00866.

AUTHOR INFORMATION

Corresponding Authors

*E-mail: peter.wells@rc-harwell.ac.uk.
*E-mail: emma.gibson@rc-harwell.ac.uk.

Author Contributions

The manuscript was written through contributions of all authors. All authors have given approval to the final version of the manuscript.

Funding

The UK Catalysis Hub is kindly thanked for resources and support provided via our membership of the UK Catalysis Hub Consortium and funded by EPSRC (portfolio grants EP/K014706/1, EP/K014668/1, EP/K014854/1, EP/K014714/1, and EP/I019693/1). The EPSRC are also thanked for the strategic equipment grant for the combined XAFS/DRIFTS setup (EP/K005030/1). A.M.B. thanks the EPSRC (EP/K007467/1). We thank UCL for the studentship for S.M.R., and the EPSRC (EP/G036675/1) for financial support of A.G. under the Centres for Doctoral Training scheme.

Notes

The authors declare no competing financial interest.

ACKNOWLEDGMENTS

The authors acknowledge the Diamond Light Source for provision of beamtime (SP8071). The RCaH are also acknowledged for use of facilities and support of their staff. P.W. thanks Prof. John Evans for continued support and guidance.

ABBREVIATIONS

DRIFTS, diffuse reflectance infrared Fourier transform spectroscopy
EXAFS, extended X-ray absorption fine structure
XANES, X-ray absorption near-edge structure
TEM-EDX, transmission electron microscopy−energy-dispersive X-ray spectroscopy
XAFS, X-ray absorption fine structure

REFERENCES

(1) Han, Y.-F.; Wang, J.-H.; Kumar, D.; Yan, Z.; Goodman, D. W.; Wayne, D. *J. Catal.* **2005**, *232*, 467−475. Gao, F.; Goodman, D. W. *Chem. Soc. Rev.* **2012**, *41*, 8009−8020.
(2) Chen, M.; Kumar, D.; Yi, C.-W.; Goodman, D. W. *Science* **2005**, *310*, 291−293.
(3) Bianchi, C. L.; Canton, P.; Dimitratos, N.; Porta, F.; Prati, L. *Catal. Today* **2005**, *102−103*, 203−212. Ketchiea, W. C.; Murayamab, M.; Davis, R. J. *J. Catal.* **2007**, *250*, 264−273.
(4) Landon, P.; Collier, P. J.; Papworth, A. J.; Kiely, C. J.; Hutchings, G. J. *Chem. Commun.* **2002**, No. 18, 2058−2059. Landon, P.; Collier, P. J.; Carley, A. F.; Chadwick, D.; Papworth, A. J.; Burrows, A.; Kiely, C. J.; Hutchings, G. J. *Phys. Chem. Chem. Phys.* **2003**, *5*, 1917−1923. Ham, H. C.; Hwang, G. S.; Han, J.; Nam, S. W.; Lim, T. H. *J. Phys. Chem. C* **2009**, *113*, 12943−12945.
(5) Enache, D. I.; Edwards, J. K.; Landon, P.; Solsona-Espriu, B.; Carley, A. F.; Herzing, A. A.; Watanabe, M.; Kiely, C. J.; Knight, D. W.; Hutchings, G. J. *Science* **2006**, *311*, 362−365.
(6) Haruta, M. *Catal. Today* **1997**, *36*, 153−166.
(7) Kung, M. C.; Davis, R. J.; Kung, H. H. *J. Phys. Chem. C* **2007**, *111* (32), 11767−11775.

DOI: 10.1021/acs.chemmater.5b00866
Chem. Mater. 2015, 27, 3714−3720

(8) Green, I. X.; Tang, W.; Neurock, M.; J. T, Y., Jr. *Science* **2011**, *333*, 736−739.
(9) Edwards, J. K.; Parker, S. F.; Pritchard, J.; Piccinini, M.; Freakley, S. J.; He, Q.; Carley, A. F.; Kiely, C. J.; Hutchings, G. J. *Catal. Sci. Technol.* **2013**, *3*, 812−818.
(10) Zhang, H.; Toshima, N. *Catal. Sci. Technol.* **2013**, *3*, 268−278.
(11) Xu, J.; White, T.; Li, P.; He, C.; Yu, J.; Yuan, W.; Han, Y.-F. *J. Am. Chem. Soc.* **2010**, *132*, 10398−10406.
(12) Tao, F.; Grass, M. E.; Zhang, Y.; Butcher, D. R.; Renzas, J. R.; Liu, Z.; Chung, J. Y.; Mun, B. S.; Salmeron, M.; Somorjai, G. A. *Science* **2008**, *322*, 932−934. Yoshida, H.; Kuwauchi, Y.; Jinschek, J. R.; Sun, K.; Tanaka, S.; Kohyama, M.; Shimada, S.; Haruta, M.; Takeda, S. *Science* **2012**, *335*, 317−319.
(13) Gao, F.; Wang, Y.; Goodman, D. W. *J. Phys. Chem. C* **2009**, *113* (33), 14993−15000.
(14) Marx, S.; Krumeich, F.; Baiker, A. *J. Phys. Chem. C* **2011**, *115*, 8195−2025.
(15) Hugon, A.; Delannoy, L.; Krafft, J.-M.; Louis, C. *J. Phys. Chem. C* **2010**, *114*, 10823−10835. Han, Y.-F.; Zhong, Z.; Ramesh, K.; Chen, F.; Chen, L.; White, T.; Tay, Q.; Yaakub, S. N.; Wang, Z. *J. Phys. Chem. C* **2007**, *111*, 8410−8413.
(16) Delannoy, L.; Giorgio, S.; Mattei, J. G.; Henry, C. R.; Kolli, N. E.; Methivier, C.; Louis, a. C. *ChemCatChem.* **2013**, *5*, 2707−2716.
(17) Newton, M. A.; Jyoti, B.; Dent, A. J.; Fiddy, S. G.; Evans, J. *Chem. Commun.* **2004**, 2382−2383.
(18) Kubacka, A.; Martínez-Arias, A.; Fernández-García, M.; Michiel, M. D.; Newton, M. A. *J. Catal.* **2010**, *270*, 275−284. Becker, E.; Carlsson, P.-A.; Kylhammar, L.; Newton, M. A.; Skoglundh, M. *J. Phys. Chem. C* **2011**, *115*, 944−951.
(19) Gaudet, J. R.; de la Riva, A.; Peterson, E. J.; Bolin, T.; Datye, A. K. *ACS Catal.* **2013**, *3* (5), 846−855.
(20) Biella, S.; Prati, L.; Rossi, M. *J. Catal.* **2002**, *206*, 242−247. Rogers, S. M.; Catlow, C. R. A.; Chan-Thaw, C. E.; Gianolio, D.; Gibson, E. K.; Gould, A.; Nan, J.; Logsdail, A.; Palmer, R.; Prati, L.; Dimitratos, N.; Villa, A.; Wells, P. P. **2015**, submitted.
(21) Marinkovic, N. S.; Wang, Q.; Barrio, L.; Ehrlich, S. N.; Khalid, S.; Cooper, C.; Frenkel, A. I. *Nucl. Instrum. Methods Phys. Res., Sect. A* **2011**, *649*, 204−206.
(22) Newville, M. *J. Synchrot. Radiat.* **2001**, *8*, 322−324.
(23) Ravel, B.; Newville, M. *J. Synchrot. Radiat.* **2005**, *12*, 537−541.
(24) Dalba, G.; Fornasini, P. *J. Synchrotron Rad.* **1997**, *4*, 243−255.
(25) Keating, J.; Sankar, G.; Hyde, T. I.; Kohara, S.; Ohara, K. *Phys. Chem. Chem. Phys.* **2013**, *15*, 8555−8565.
(26) Dash, P.; Bond, T.; Fowler, C.; Hou, W.; Coombs, N.; Scott, R. W. J. *J. Phys. Chem. C* **2009**, *113*, 12719−12730.
(27) Bokhoven, J. A. v.; Miller, J. T. *J. Phys. Chem. C* **2007**, *111*, 9245−9249.
(28) Marx, S.; Baiker, A. *J. Phys. Chem. C* **2009**, *113*, 6191−6201.
(29) Teng, X.; Wang, Q.; Liu, P.; Han, W.; Frenkel, A. I.; Wen, W.; Marinkovic, N.; Hanson, J. C.; Rodriguez, J. A. *J. Am. Chem. Soc.* **2008**, *130*, 1093−1101.
(30) Newton, M. A.; Michiel, M. D.; Kubacka, A.; Fernandez-Garcia, M. *J. Am. Chem. Soc.* **2010**, *132*, 4540−4541.
(31) Deplanche, K.; Merroun, M. L.; Casadesus, M.; Tran, D. T.; Mikheenko, I. P.; Bennett, J. A.; Zhu, J.; Jones, I. P.; Attard, G. A.; Wood, J.; Selenska-Pobell, S.; Macaskie, L. E. *J. R. Soc. Interface* **2012**, *9*, 1705−1712.
(32) McKale, A. G.; Veal, B. W.; Paulikas, A. P.; Chan, S.-K. *Phys. Rev. B* **1988**, *38* (15), 10919−10921.
(33) Andrew, M.; Beale, B. M. W. *Phys. Chem. Chem. Phys.* **2010**, *12*, 5562−5574.
(34) Frenkel, A. I.; Wang, Q.; Sanchez, S. I.; Small, M. W.; Nuzzo, R. G. *J. Chem. Phys.* **2013**, *138*, 064202−064207.
(35) Hadjiivanov, K. I.; Vayssilov, G. N. *Adv. Catal.* **2002**, *47*, 307−511.
(36) Ruggiero, C.; Hollins, P. *J. . Chem. Soc., Faraday Trans.* **1996**, *92* (23), 4829−4834.
(37) Giorgi, J. B.; Schroeder, T.; Baumer, M.; Freund, H.-J. *Surf. Sci.* **2002**, *498*, L71−L77. Sheppard, N.; Nguyen, T. T., The Vibrational Spectra of Carbon Monoxide Chemisorbed on the Surfaces of Metal Catalysts-A Suggested Scheme of Interpretation. In *Advances in Infrared and Raman Spectroscopy*, Clark, R. J. H.; Hester, R. E., Eds.; Heyden & Son: London, 1978; Vol. *5*, pp 67−148.
(38) Grunwaldt, J.-D.; Maciejewski, M.; Becker, O. S.; Fabrizioli, P.; Baiker, A. *J. Catal.* **1999**, *186* (2), 458−469.
(39) Bowker, M. *Chem. Soc. Rev.* **2008**, *37*, 2204−2211.

DOI: 10.1021/acs.chemmater.5b00866
Chem. Mater. 2015, 27, 3714−3720